ARTICLE NO. 78-1350R

Atmospheric Flight of a Variable-Bend Body

William J. Larkin* and Mitchell Thomas†
L'Garde, Inc., Newport Beach, Calif.

The concept discussed is that of steering a flying vehicle by bending its body. The analysis presented shows that the variable-bend body control technique is of special value where the system can be designed so that each element of the body roughly carries its own weight. Under these conditions hinge moments at the body's bend can be made low while high performance is obtained. Furthermore, hinge moments remain low even when thrust vectoring is added to the system, while the versatility of the control system is increased. The analysis delineates the conditions needed for a thrusting bent body to attain optimum performance. Examples are given for a high-g maneuvering surface-to-air missile illustrating the low hinge moments required.

Nomenclature

CL_{max} = maximum value of lift coefficient for a given body
CM = center of mass location
CP = aerodynamic center of pressure location
C_m = aerodynamic pitching coefficient around CM, rad^{-1}
C_{x_0} = drag coefficient
C_z = aerodynamic normal force coefficient, rad^{-1}
F = rocket thrust, lb
$\bar{F}$ = F/QS
F_x, F_z = total vehicle forces in x and z directions, lb
F_I = inertia force, lb
F_L = lift force, lb
K = amplification factor = α/δ
m = mass, slugs; subscripts 1 and 2 refer to forebody and aftbody, respectively
$\bar{m}_i$ = mass fraction = m_i/m
N_H = hinge moment; torque on hinge joint, ft-lb
N_y = moment about CM, ft-lb
Q = dynamic pressure, lb/ft^2 or klb/ft^2
R_B = base radius, ft
R_n = nose radius, ft
S = vehicle aerodynamic reference area, ft^2
S_1 = forebody aerodynamic reference area, ft^2
t = time of flight, s
v = velocity, ft/s
x_a = coordinate of total vehicle CP, ft
x_{a1}, x_{a2} = distance from pivot to fore- and aftbody CP's, ft
x_j = coordinate of joint (hinge), ft
x_L = vehicle body length, ft
x_0 = coordinate of the total vehicle CM, ft
x_{01} = coordinate of forebody CM, ft
x_{02} = distance from aftbody CM to pivot point, ft
x_p = coordinate of pivot point, ft
$\bar{x}$ = x as defined by subscript above, nondimensionalized by dividing by x_L
z_0 = vertical coordinate of total vehicle CM
α = forebody angle of attack; subscript T for trimmed condition
δ = tail deflection angle relative to forebody; subscript T for trimmed condition
$\bar{\Delta}$ = total body static margin (fraction of vehicle length)
Δ_1, Δ_2 = fore- and aftbody static margins, ft
λ = R_n/R_B

Received July 25, 1978; presented as Paper 78-1350 at the 1978 AIAA Atmospheric Flight Mechanics Conference, Palo Alto, Calif., Aug. 8, 1978; revision received Jan. 8, 1979.

Index category: LV/M Dynamics and Control.

*Director. Member AIAA.
†President. Associate Fellow AIAA.

Switchtail Control Principle

THE purpose of this paper is to present a brief synopsis of the status of bent-body control (switchtail) to serve as an introduction to the concept. The technique, to our knowledge, has not previously been documented in the open technical literature.

To bend the body in order to provide aerodynamic moments for steering can be considered a "natural" system in that the actuation forces required can be made negligible. Figure 1 shows the switchtail control concept compared to a more conventional canard surface. The essential element of the switchtail control is that the sections of the body should be designed so that each section may carry its own weight. Analysis then shows that design conditions can be found, independent of the flight environment, where the sum of all torques around the hinge point is zero for steady-stage high-acceleration turning. This basic property of the switchtail control produces a variety of advantageous features that are not offered by any other control system. The simplicity and power of switchtail control promises a highly reliable and effective missile, with low weight and cost.

Advantages of Switchtail Control

Key advances with switchtail control (with illustrations from some earlier studies) are the following:

1) The inertial load from the mass of the tail tends to balance the lift load on the tail during maneuvers, permitting reasonable control system actuation weights for vehicles designed for a high static-margin and lift-acceleration requirement. Figure 2 shows early calculations of the hinge-torque-to-lift ratio as a function of aftbody and forebody static margin (Δ_2 and Δ_1, respectively). These data are for steady-state turning and do not include the minimum forces that would be required for any real mechanization. For the line $N_H/F_L = 0$, the inertial and aerodynamic forces are equal. Figures 3 and 4 show the aerodynamic and angle-of-attack characteristics for a maneuvering re-entry vehicle (MaRV) designed at point "X" on Fig. 2.

2) A high static margin combined with the "clean" switchtail configuration (linear areodynamics) simplifies the

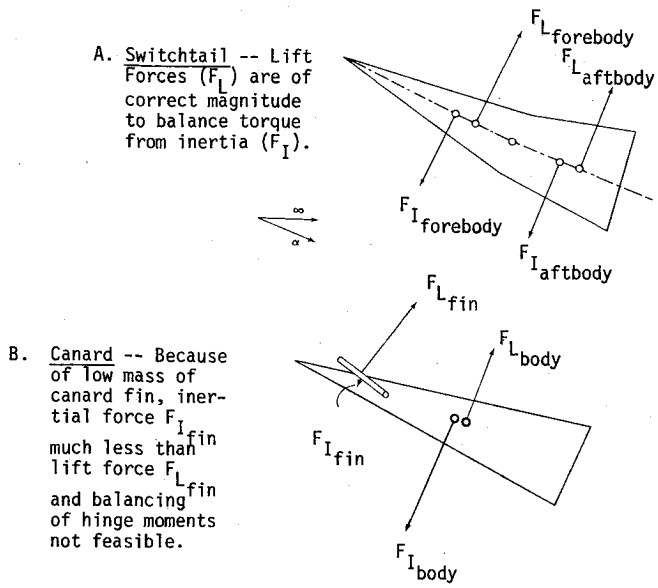

Fig. 1 Switchtail/canard comparison.

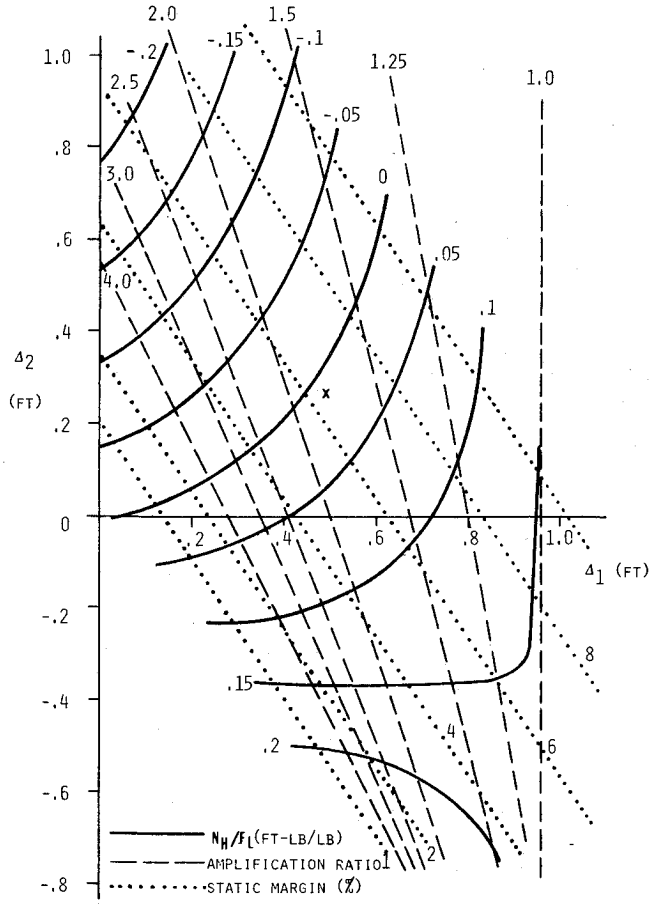

Fig. 2 Acutator torque requirements for 80% pivot switchtail.

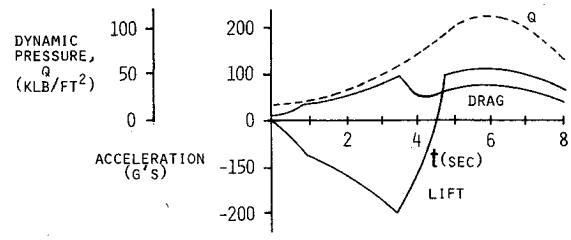

Fig. 3 Typical switchtail MaRV performance.

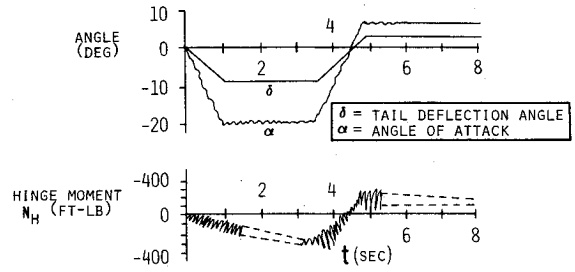

Fig. 4 Hinge performance for typical switchtail MaRV.

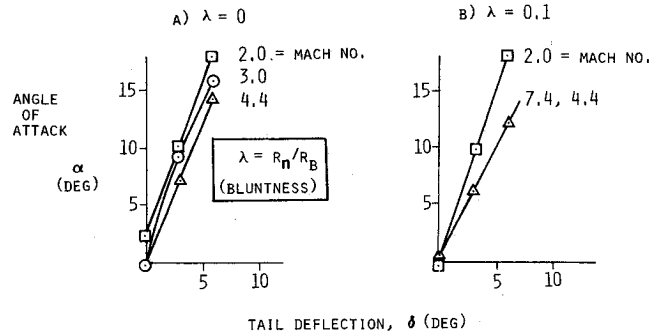

Fig. 5 Linearity of trim-angle control; wind-tunnel data for 9-deg cone, 80% pivot.

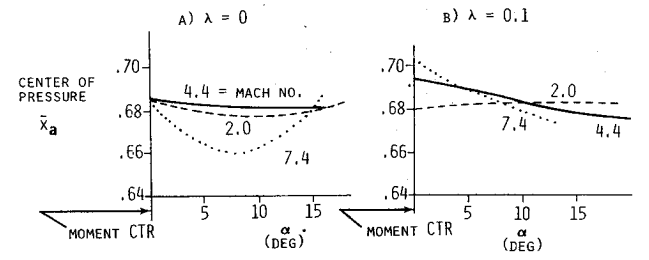

Fig. 6 Stability of MaRV switchtail during trim and bluntness changes.

control system design and reduces the sensitivity of the control system to nose blunting and other vehicle shape changes. Linearity of control is seen in the data of Fig. 5. Considerable nose shape change can occur without instability occurring, as in Fig. 6.

3) Windward control permits high vehicle-angle-of-attack capability (up to CL_{max} if desired) at response rates approaching the natural pitch frequency of the vehicle without exceeding steady-state trim actuation loads. Recent efforts on the Switchtail Interceptor Missile (SWIM) Concept Evaluation Study demonstrating these points follow:

Figures 7-9 show numerical simulations of the SWIM-study high-performance interceptor, plotted automatically by a computer code. Figure 7 shows the commanded tail deflections, the resulting tail deflection, and the subsequent angle-of-attack history flown by SWIM. Figure 8 shows the resulting lateral-g history—the ability to perform a switchover maneuver (from a high-g steady turn to a high-g steady turn in the opposite direction) in about 0.1 s. Figure 9 shows calculated hinge moments in ft-lb on the actuators and they are seen to be less than 10,000 ft-lb, well within current capability of available light actuators. Furthermore, the forces required to keep the missile in a steady high-acceleration turn settle down to be near zero, as predicted for a good switchtail design.

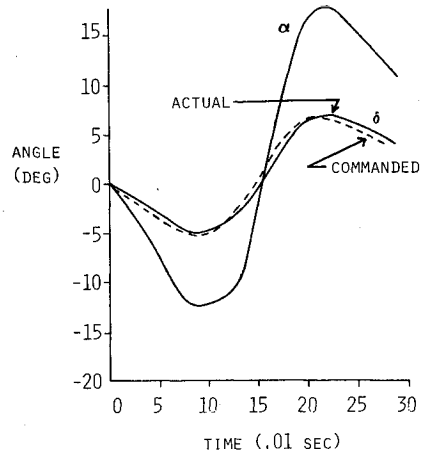

Fig. 7 Tail deflection history—SWIM.

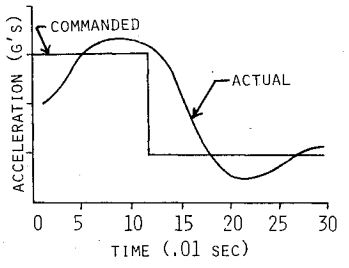

Fig. 8 Acceleration history—SWIM.

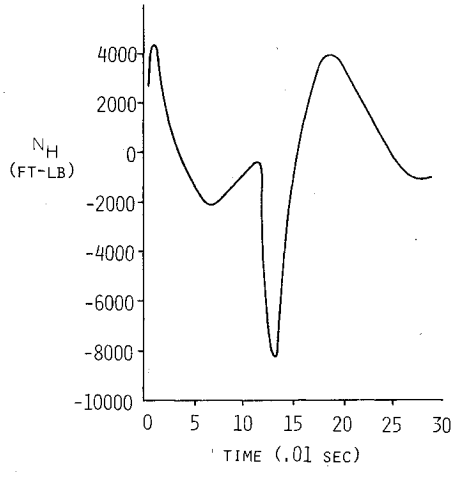

Fig. 9 Hinge-moment history—SWIM.

Aerodynamic Characteristics and Control Effectiveness

In any switchtail missile design the maneuver level and response requirements, together with the flight conditions over which the system must operate, dictate the lift force and control system response requirements. The latter, in turn, influence the angle-of-attack and control effectiveness requirements.

The essential features of the switchtail aerodynamic characteristics can be obtained from linearized analysis. In the linear range of the angle of attack α and the tail deflection angle δ, the aerodynamic normal force coefficient and the pitching moment coefficient about CM may be written in the form

$$C_z = C_{z_\alpha}\alpha + C_{z_\delta}\delta \tag{1}$$

$$C_m = C_{m_\alpha}\alpha + C_{m_\delta}\delta \tag{2}$$

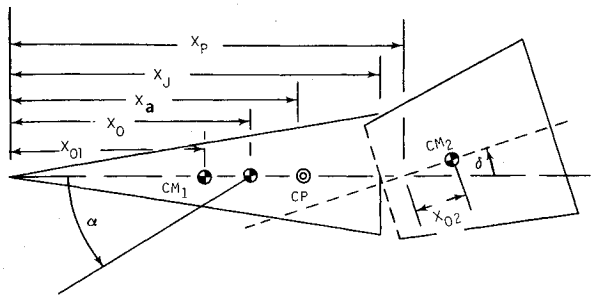

Fig. 10 Switchtail configuration terminology.

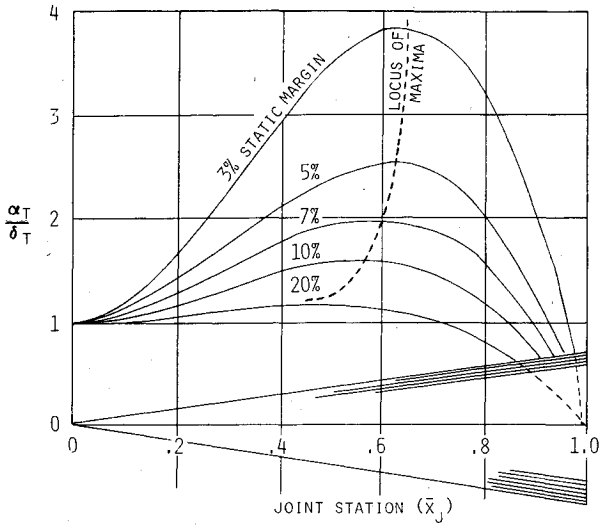

Fig. 11 Theoretical trim amplification, sharp-cone switchtail.

Using Newtonian aerodynamic arguments and neglecting the small moment contribution of the axial force component about the vertical CM offset caused by tail deflection, it can be shown that

$$C_{z_\delta} \simeq -(1-\bar{x}_j^2)C_{z_\alpha} \tag{3}$$

$$C_{m_\alpha} = -\bar{\Delta}C_{z_\alpha} \tag{4}$$

$$C_{m_\delta} \simeq C_{z_\alpha}[\bar{\Delta} + \bar{x}_0\bar{x}_j^2 - \bar{x}_a\bar{x}_j^3] \tag{5}$$

where $\bar{\Delta}$ denotes the static margin, and $\bar{x}_0$, $\bar{x}_a$, and $\bar{x}_j$ denote the nondimensional locations of the vehicle CM, center of pressure, and hinge joint, respectively (see Fig. 10). The origin of coordinates is taken as the vehicle's nose; a "bar" over a dimension means it has been divided by vehicle length.

For the switchtail concept, a measure of the control effectiveness is the trim angle of attack available for a given tail deflection. Using the previously derived equations, it has been shown that the amplification factor K is

$$K = \frac{\alpha_T}{\delta_T} \simeq \frac{\bar{\Delta} + \bar{x}_0\bar{x}_j^2 - \bar{x}_a\bar{x}_j^3}{\bar{\Delta}} \tag{6}$$

Also for a given $\bar{x}_a$ and $\bar{x}_0$, $K_{\max}$ occurs at $\bar{x}_j = \frac{2}{3}(\bar{x}_0/\bar{x}_a)$.

A plot of K as a function of $\bar{x}_j$ for different static margins of a 9 deg sharp cone is shown in Fig. 11. The results indicate that in the primary range of design interest, i.e., $0.6 < \bar{x}_j < 0.8$, $0.03 < \bar{\Delta} < 0.06$, amplification factors in the range of 1.8 to 3.8 are available.

The maneuver performance of the switchtail may be assessed by considering the trimmed normal force. Using the

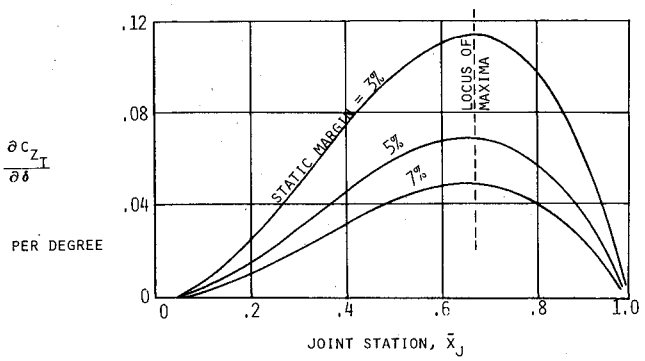

Fig. 12 Theoretical net trim normal force per degree tail deflection for a sharp-cone switchtail.

previous simplifying assumptions, it has been shown that

$$C_{z_T} \simeq C_z \frac{\bar{x}_a(\bar{x}_j^2 - \bar{x}_j^3)\delta_T}{\bar{\Delta}} \tag{7}$$

or the maneuvering capability of the switchtail per unit tail deflection can be expressed as

$$\frac{\partial C_{z_T}}{\partial \delta_T} = C_{z_{T\delta}} = \frac{C_{z_\alpha}}{\bar{\Delta}} \bar{x}_a(\bar{x}_j^2 - \bar{x}_j^3) \tag{8}$$

$C_{z_{T_\delta}}$ is plotted in Fig. 12. It may be noted that for a given center of pressure and CM locations, $C_{z_{T\delta}}$ has a maximum at $\bar{x}_j = \frac{2}{3}$ and is not overly sensitive to body joint location. Thus, off-optimum joint locations to the extent of 0.05 to 0.1 body length do not seriously degrade the maneuver performance of the switchtail.

Addition of Thrust to the Vehicle

If the aftbody of the bent vehicle contains an axial-thrust rocket motor, an additional turning moment is produced that augments the aerodynamic forces. Although briefly analyzed for a specific configuration during the SWIM study, the thrust vector effect remained essentially unexplored until now. This section contains an analysis aimed at illustrating the significant features of a dual thrust/aero bent-body control system.

The bent-body control system computer code was modified to include thrusting. The resulting code includes the effects of thrust and also the loss of propellant mass and shifting of the center of mass. Coriolis terms and damping terms are included in the full equations as developed by Pottsepp.[1]

The detailed equations of motion were simplified to determine the steady-state trimmed-flight conditions, as has been done earlier for the case without thrust. For small trim angles, assuming that gravitational, damping, mass-loss, and other higher order terms can be neglected, the equations of motion for the thrusting bent body become the following (refer to Fig. 10).

Moments around CM:

$$N_y = 0 = QSx_L(C_{m_\alpha}\alpha + C_{m_\delta}\delta) + F(x_p - x_0)\delta - \dot{m}_2 x_{02}\delta F_x \tag{9}$$

where

$$F_x = QSC_{x_0} - F$$

Hinge Moments:

$$N_H = (x_{0l} - x_p)F_z + QS_l C_{z_{\alpha l}} x_{al}\alpha \tag{10}$$

where

$$F_z = QS(C_{z_\alpha}\alpha + C_{z_\delta}\delta) - F\delta$$

Table 1 Characteristics of reference vehicle used in calculations reference vehicle is 9-deg half-angle cone

$x_L = 5.75$ ft, $x_j = 4.6$ ft (80%), $R_B = 0.91$ ft
$m = 350$ lb, $m_l = 222$ lb, $C_{z_\alpha} = 1.98$, $C_{x_0} = 0.055$
$x_{al} = 0.317\,x_j$, $x_{a2} = 0.707\sqrt{x_L^2 + x_j^2} - x_j$
$x_a = 0.683 x_L$

Table 2 Typical values of normalized thrust

Altitude, ft	v, kft/s	Q, lb/ft^2	QS, lb	a, g	$\bar{F}$
10,000	1	1755	4545	10	0.6
100,000	15	7465	19,336	10	0.18
...	...	100,000	250,000	500	0.56

and

$C_{z_{\alpha l}}$ = normal force coefficient of forebody ($\simeq C_{z_\alpha}$)

In the following calculations the baseline vehicle has the characteristics given in Table 1.

Equation (9) defines the conditions required for steady trimmed flight. The amplification factor is then

$$\frac{\alpha}{\delta} \equiv K = \frac{x_L C_{m_\delta} + \bar{F}(x_p - x_0 + \dot{m}_2 x_{02}) - \dot{m}_2 x_{02} C_{x_0}}{-x_L C_{m_\delta}} \tag{11}$$

For the case without thrust the amplification factor was seen to be independent of flight conditions, depending only on the vehicle design parameters. With thrust included, the amplification ratio is a function of thrust and dynamic pressure. Defining the ratio of thrust to dynamic force as $\bar{F}$, the effect of this ratio on the amplification factor is shown in Fig. 13 for the reference vehicle. The primary effect of thrusting is to push the vehicle trim angle to a higher value, thus increasing the available maneuver force.

Typical values of $\bar{F}$ are presented in Table 2 for a vehicle mass $\simeq 250$ lb and $C_x \simeq 0.055$.

For $\bar{F}$ increasing, K becomes proportional to $\bar{F}$. The linearized analysis used becomes invalid, and steady-stage trimming is not possible, for $\bar{F}$ sufficiently large.

The hinge moments can be normalized by dividing by the normal force F_z. The resulting expression obtained by combining Eqs. (10) and (11) is

$$\frac{N_H}{F_z} = \frac{\dot{m}_l(x_p - x_{0l})(C_{z_\alpha}K + C_{z_\delta} - \bar{F}) - (S_l/S)C_{z_{\alpha l}}x_{al}K}{C_{z_\alpha}K + C_{z_\delta} - \bar{F}} \tag{12}$$

Data for the case of no thrusting and the reference vehicle are compared to similar data generated earlier (see Fig. 2). The comparison shown in Fig. 14 shows that the agreement is generally good. Differences are most likely due to the different normalized factor used and slightly different coordinates for the center of pressure. The range of interest is defined by the area including the lines of N_H/F_z. The lengths of these lines are limited by the conditions that the center of mass of either vehicle section must be somewhere in that section. That is, points beyond the lines shown correspond to physically unrealistic vehicle configurations. Solutions to Eq. (12) for the reference vehicle, for mass loss = 0, are presented in Fig. 15. For a given forebody static margin (Δ_1) the effect of thrust on the minimum torque design is to require a smaller aft body static margin (Δ_2) for increasing thrust.

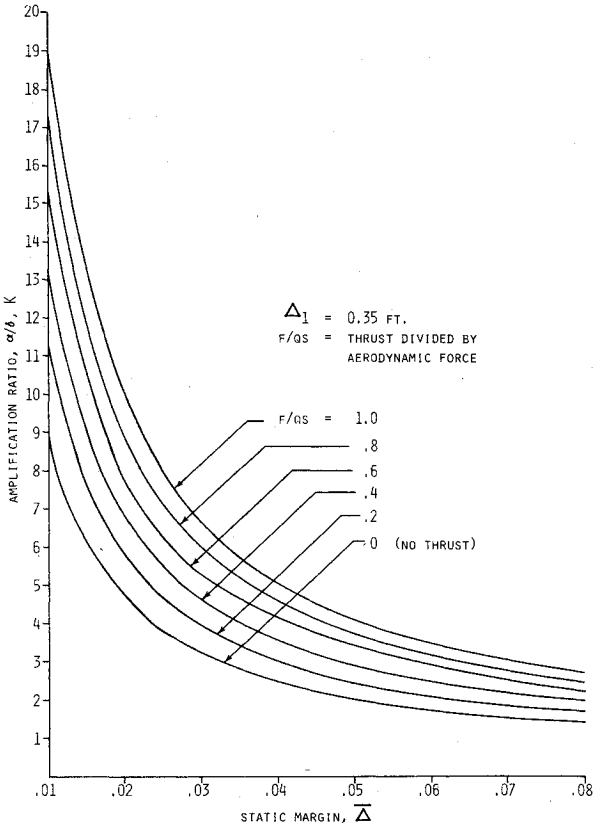

Fig. 13 Increase of trim angle with thrust addition.

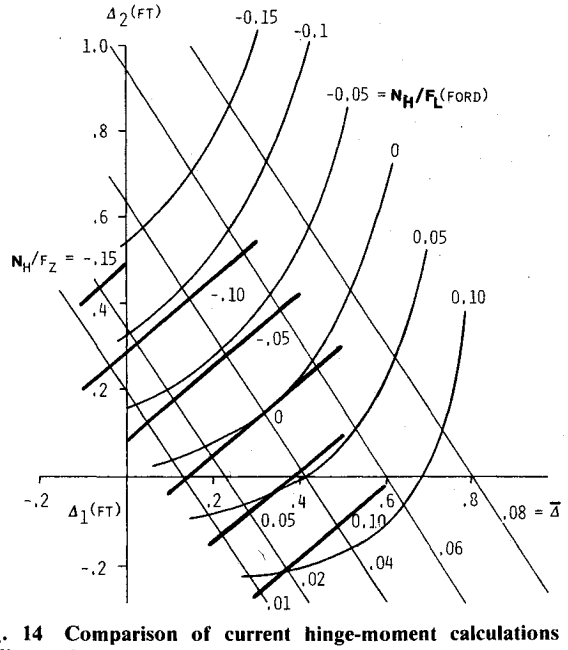

Fig. 14 Comparison of current hinge-moment calculations with earlier work.

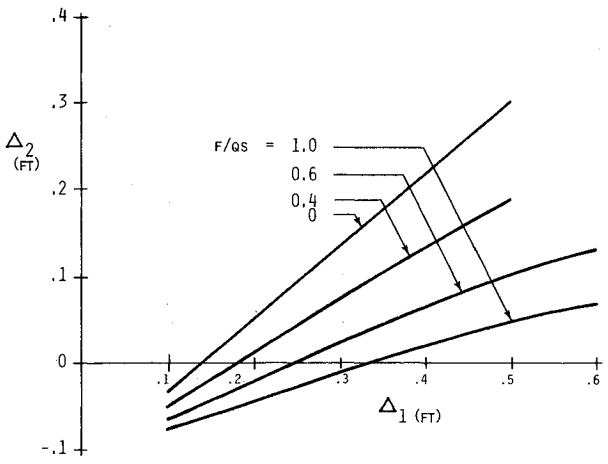

Fig. 15 Lines of zero hinge moment for various thrust levels.

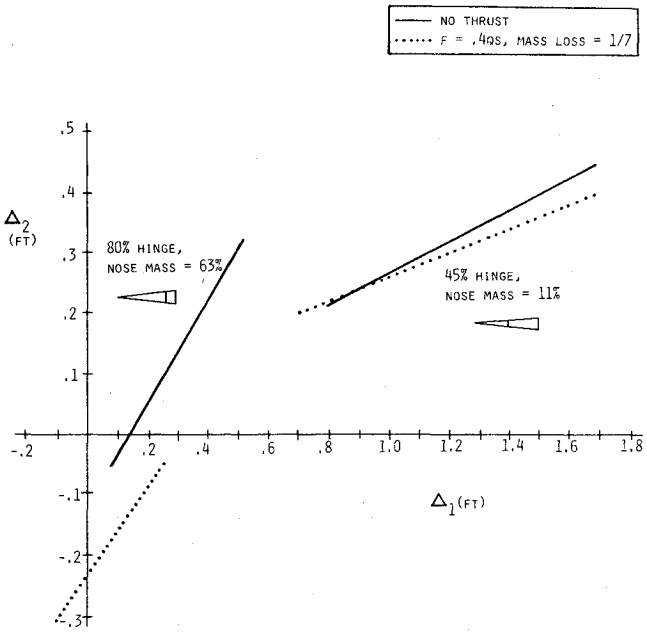

Fig. 16 Hinge-moment lines for vehicle including propellant mass loss.

The data of Fig. 15 are valid for the reference vehicle at any point in time; however, since the mass of the vehicle will be changing, a more meaningful comparison is given in Fig. 16. The two lines near the Δ_2 axis compare the reference vehicle at zero thrust to the same vehicle with $\bar{F}=0.4$ and total weight reduced from 350 to 300 lb. As mentioned earlier, the lengths of the lines shown are significant; extrapolations of the line beyond that shown will result in unrealistic or impossible vehicle configurations. The reference vehicle, therefore, if it were to lose about 50 lb of propellant, as in this example, should be designed with forebody static margins from about 0.1 to 0.25 ft, so that a transition is possible from the $F=0$ to the $F=0.4$ curves as Δ_2 changes during engine firing to minimize the hinge moments.

In this example an imbalance will occur when the motor is initially fired unless static margin is actively controlled to make an abrupt transition from the no-thrust to the thrusting curve. However, designs are possible such that abrupt changes do not occur. The curves on Fig. 16 for a modified version of the reference vehicle with its joint moved up to a coordinate 0.45 x_L show that solutions are available where the problem of minimizing hinge torques is itself minimized. For practical purposes, a vehicle designed with Δ_1 anywhere from 0.9 to 1.7 ft will have minimum hinge moments after losing 50 lb while thrusting at $\bar{F}=0.4$, if it had initially been designed to have minimum moments at zero thrust, and if aftbody static margin can be held constant.

Design optimization includes, at least, design trades between vehicle performance and hinge-actuator size to give the lowest weight system still meeting performance goals. Although guidelines for design can be deduced from the sort of analysis presented above, preliminary optimized designs

can be found only by parametric studies of flight simulations over a large range of vehicle design parameters (Δ_1, Δ_2, m_1, m_2, x_j) using Monte Carlo trajectory analysis.

Acknowledgments

This work was supported in part by the Ballistic Missile Defense Advanced Technology Center under Contract DASG60-76-C-0072, and in part by L'Garde, Inc. Thanks are due L. Pottsepp who generated the basic equations used throughout the analysis and D. Hender who programmed the dynamics codes. The important issues that were relevant to the SWIM study were pointed out by the BMDATC program engineer, R. Riviere. Also much of the early data generated relative to this concept and sampled in this paper were created at Ford Aerospace and Communications Corporation by numerous individuals, including A.R. Hirasuna, M.W. Hoyt, W.L. Francis, R. Grabow, E.M. Schafer, R.R. Auelmann, J. Dowdy, and R. Irwin.

References

[1] Pottsepp, L. and Lebovitz, N.R., "A General Formulation of the Equations of Motion of a Missile," Douglas Aircraft Co., Santa Monica, Calif., SM-49217, Dec. 1965.